Supplement of Atmos. Chem. Phys., 26, 983–999, 2026
https://doi.org/10.5194/acp-26-983-2026-supplement

Atmospheric Chemistry and Physics
Open Access
EGU

Supplement of

Transported African Dust in the Lower Marine Atmospheric Boundary Layer is Internally Mixed with Sea Salt Contributing to Increased Hygroscopicity and a Lower Lidar Depolarization Ratio

Sujan Shrestha et al.

Correspondence to: Robert E. Holz (reholz@ssec.wisc.edu) and Cassandra J. Gaston (cgaston@miami.edu)

S1. Overview of Airborne Aerosol Sampling

The Center for Interdisciplinary Research Projects in Airborne Science (CIRPAS), operated by the Naval Postgraduate School (NPS), provides a specialized Twin Otter research aircraft designed to support environmental and atmospheric science missions. The Twin Otter is a versatile aircraft well-suited for research flights enabling direct sampling of the lower troposphere. Equipped with multiple wing pylons, fuselage ports, and integrated power systems, the aircraft can accommodate a wide range of meteorological and aerosol instrumentation. CIRPAS adheres to rigorous calibration protocols and offers comprehensive logistical support to ensure high-quality data acquisition across multi-institutional field campaigns.

In situ measurements of air temperature (Rosemount total temperature probe, model E102AL) (Friehe and Khelif, 1992) and dew point temperature (Vigilant Chilled Mirror Hygrometer, Edgetech Instruments Inc., Hudson, MA) were used by flight scientists to determine the cloud base height (CBH). During the initial sounding at each sampling station, vertical profiles of air temperature and dewpoint temperature were monitored as they gradually converged with increasing altitude. The CBH was identified as the first significant maximum in RH, typically between 90-100% RH and the onset of condensation. This ascent or descent profiling strategy was performed during each flight to establish sampling levels and capture the vertical moisture structure critical for identifying the cloud base.

Aerosol measurements aboard the CIRPAS Twin Otter rely on the characterization of aerosol sampling dynamics. The aircraft's aerosol inlet has been evaluated under both flight and wind tunnel conditions to quantify its transmission efficiency across a range of particle sizes. Studies show that the inlet's transmission efficiency begins to decline near 3.5 μm particle

diameter but stabilizes at 5.5 μm with a transmission efficiency just above 0.6 for particles up to 9 μm (Hegg et al., 2005). This behavior is likely attributed to sub-isokinetic aspiration flow, wherein the inlet flow velocity is lower than the freestream velocity, leading to inertial losses of larger particles.

S2. Single Particle Aerosol Composition and Size Distribution

Single-particle chemical composition and morphology of aerosol samples collected during dust events were examined using computer-controlled scanning electron microscopy with energy-dispersive X-ray spectroscopy (CCSEM/EDX). The analysis revealed a diverse set of particle types with distinct chemistries and morphologies, including mineral dust, sea spray, aged sea spray, internally mixed mineral dust and sea spray, sulfates, and organics (Ault et al., 2014; Royer et al., 2023). Representative scanning electron microscopy (SEM) images and corresponding EDX spectra for each particle class are shown in Fig. 4a in main text.

Mineral Dust: Mineral dust particles were primarily characterized by the presence of aluminosilicate elements such as Si, Al, Fe, K, Ca, and Mg, consistent with long-range transported Saharan dust (Reid et al., 2003; Royer et al., 2023, 2025; Twohy et al., 2009; Levin et al., 2005; Krueger et al., 2004; Hand et al., 2010; Denjean et al., 2015). Notably, approximately only 25% of the dust particles analyzed contained sulfur and nitrogen, suggesting atmospheric chemical aging either during transport or during entrainment into the marine boundary layer (MBL). This is consistent with earlier findings at the site that reported minimal evidence of aging in mineral dust (Kandler et al., 2018; Royer et al., 2025).

Sea Spray and Aged Sea Spray: Fresh sea spray particles were identified by a high relative abundance of Na and Cl and exhibited crystalline morphologies indicative of halite (NaCl). Small peaks of Mg further confirmed their marine origin. Aged sea spray particles were

distinguished by depleted chloride content and enriched sulfur and nitrogen signatures, likely resulting from heterogeneous reactions with atmospheric acidic gases such as sulfuric acid (H_2SO_4), nitric acid (HNO_3), and dinitrogen pentoxide (N_2O_5). These interactions are known to produce Cl-depleted sea spray and form secondary aerosol (Ault et al., 2013a; Royer et al., 2023, 2025; Gaston et al., 2011).

Internally Mixed Mineral Dust and Sea Spray: These particles exhibited a heterogeneous composition, containing both dust-derived (Si, Al, Fe, K, Ca, Mg) and marine-derived (Na, Cl) components (Royer et al., 2023, 2025; Kandler et al., 2018). Elemental distributions varied within individual particles, indicating spatially localized mixing of the two sources. The generally low percentage of nitrogen and sulfur suggests limited atmospheric aging of this particle type. This is contrary to wintertime observations at Barbados by Royer et al. (2025), where SEM/EDX elemental mapping showed that signs of aging, such as the presence of sulfur or nitrogen, were confined to the sea spray portions of these mixed particles. Previous work at the same site proposed that this internal mixing likely occurs locally, potentially driven by turbulent interactions between airborne dust and sea spray (Kandler et al., 2018).

Organics: Organic particles were predominantly composed of carbon and oxygen (>95%), with minor contributions from inorganic constituents (<5%). Several larger particles were observed, potentially corresponding to marine gels, characterized by Mg-rich shells and sea spray-dominated cores (Ault et al., 2013b; Gaston et al., 2011). These marine gels are typically formed from bubble-bursting processes at the ocean surface, where hydrophobic organic compounds concentrated in the sea surface microlayer become aerosolized and associate with divalent cations during gel formation (Chin et al., 1998).

Sulfates: Sulfate-rich particles were identified based on dominant sulfur signals accompanied by carbon, oxygen, and nitrogen. These particles are consistent with marine secondary aerosol components such as ammonium sulfate ($(NH_4)_2SO_4$) and ammonium bisulfate (NH_4HSO_4) (Hand et al., 2010; Royer et al., 2023). The elevated carbon content suggests these particles also contain a substantial organic fraction, a common feature in marine submicron aerosols (O'Dowd and de Leeuw, 2007).

S3. Estimation of Expected Lidar Depolarization Ratio

S3.1 Modeling expected depolarization ratio mixture.

To estimate the expected aerosol depolarization ratio ($\delta_{expected}$), we begin by modeling the total aerosol backscatter as a mixture of contributions from dust and marine aerosols. The total backscatter coefficient (ν) is expressed as:

$$\nu = \nu^{(d)} + \nu^{(m)} \quad (S1)$$

where, $\nu^{(d)}$ and $\nu^{(m)}$ are dust and marine air mass backscatter, respectively.

The total parallel ($\nu_{\parallel}$) and perpendicular ($\nu_{\perp}$) components of the backscatter can be similarly expressed as:

$$\nu_{\parallel} = \nu_{\parallel}^{(d)} + \nu_{\parallel}^{(m)} \quad (S2)$$

$$\nu_{\perp} = \nu_{\perp}^{(d)} + \nu_{\perp}^{(m)} \quad (S3)$$

The depolarization ratio mixture is then defined as:

$$\delta = \frac{\nu_{\perp}}{\nu_{\parallel}} \quad (S4)$$

Using this formulation, the expected depolarization ratio can be alternatively written as:

$$\delta expected = \frac{v_{\perp}^{(d)}}{v_{\parallel}^{(d)} + v_{\parallel}^{(m)}} + \frac{v_{\perp}^{(m)}}{v_{\parallel}^{(d)} + v_{\parallel}^{(m)}} \quad (S5)$$

This formulation requires estimation of the aerosol-specific backscatter and their polarized components which are computed as described in the following sections.

S3.2 Estimating the aerosol specific polarized backscatter

To calculate the expected depolarization, we first estimate extinction β [m^{-1}] using the observed particulate backscatter (v) and lidar ratio μ [sr]:

$$\beta = \nu\mu \quad (S6)$$

Next, the aerosol specific backscatter components for marine and dust contributions are derived using their respective mass concentrations $M^{(d)}$ and $M^{(m)}$ [μg m^{-3}], and lidar ratio cut offs for dust (μ^d) and marine aerosols (μ^m) were taken as 40 and 20, respectively:

$$v^{(m)} = \frac{M^{(m)}}{M^{(m)} + M^{(d)}} \frac{\beta}{\mu^m} \quad (S7)$$

$$v^{(d)} = \frac{M^{(d)}}{M^{(m)} + M^{(d)}} \frac{\beta}{\mu^d} \quad (S8)$$

S3.3 Compute the marine and dust parallel and perpendicular backscatters

Using the campaign-derived in-situ linear depolarization ratios for dust and marine aerosols in-situ marine $\delta^{(m)}$ and dust $\delta^{(d)}$ (i.e., 0.3 for dust and 0.02 for marine), we calculate the aerosol specific backscatter into polarized components.

a. the parallel polarized marine and dust backscatters is calculated as:

$$v_{\parallel}^{(m)} = \frac{v^{(m)}}{(1 + \delta^{(m)})} \quad (S9)$$

$$v_{\parallel}^{(d)} = \frac{v^{(d)}}{(1+\delta^{(d)})} \quad (S10)$$

b. the perpendicular polarized marine and dust backscatters is calculated as:

$$v_{\perp}^{(m)} = \delta^{(m)} v_{\parallel}^{(m)} \quad (S11)$$

$$v_{\perp}^{(d)} = \delta^{(d)} v_{\parallel}^{(d)} \quad (S12)$$

Finally, the expected linear depolarization ratio is computed by substituting Eqs. (S7) – (S12) into Eq. (S5).

S4. Estimation of the Expected Lidar Depolarization Ratio with Hygroscopic Growth

Here we model the expected aerosol depolarization ratio (δ_{expected}) by taking into account the hygroscopic growth of the water-soluble aerosol (i.e., marine) particles that are mixed with non-hydrated dust particles. Hygroscopic growth describes how the particle volume increases as the particle absorbs water vapor from the air (Hänel, 1976, 1972). The volumetric growth has a large effect on the depolarization of the mixture of marine and dust particles; as the marine particle volume increases, the backscatter [m^{-1} sr^{-1}] of this particle type increases relative to the dust particle backscatter [m^{-1} sr^{-1}]. Consequently, the depolarization of the mixture of marine and dust particles is driven lower by hygroscopic growth.

Similar to Eq. (S5) the expected depolarization ratio $\delta expected$ is modeled by the weighted sum of the dust and marine (hygroscopic) particles.

$$\delta expected = \frac{v^{(d)}\delta^{(d)} + v^{(m)}\delta^{(m)}}{v^{(m)} + v^{(m)}} \quad (S13)$$

Since the HSRL 532nm wavelength is much smaller than the dust and marine particles sizes, the extinction efficiency can be approximated by a factor 2 (Hänel, 1976). Hence, the dust backscatter [m^{-1} sr^{-1}] can be modeled as

$$\nu^{(d)} = 2N_d \frac{\chi A_d}{\mu^{(d)}} \quad (S14)$$

where N_d is the number density [m^{-3}], A_d is the cross-sectional area [m^2] of dust particles and $\mu^{(d)}$ is the dust lidar ratio [sr]. The marine backscatter [m^{-1} sr^{-1}] is similarly defined

$$\nu^{(m)} = 2N_m \frac{\chi A_m}{\mu^{(m)}} \quad (S15)$$

where $\mu^{(m)}$is the marine lidar ratio [sr].The enhancement factor $\chi > 0$ models the marine aerosol extinction enhancement due to the marine particle cross-sectional area A_m increasing with increasing RH (i.e., hygroscopic growth) (Eq. (S4) in Hänel, 1972). We approximate the enhancement factor χ relative to a dry RH of RH_{ref} = 40%

$$\chi = \left(\frac{1 - RH_{ref}/100}{1 - RH/100}\right)^{2\epsilon} \quad (S16)$$

where the "fitted" exponent 2ϵ is approximately equal to 1 (Hänel, 1972). Thus, at a RH of 80% the marine aerosol extinction is approximately three times as large compared to the marine extinction at a RH of 40%, which implies that the marine aerosol backscatter is three times as large if the number density is fixed.

Before we expand the depolarization ratio $\delta expected$ formulation Eq. (S13) with the backscatter definitions Eqs. (S14) and (S15), there are a couple of approximations that we can make to simplify the formulation. First, since the RH in the MABL is approximately 80% the marine particles have taken on water, are large (relative to the laser wavelength) and spherical (Hänel,

1976). As such we can approximate the marine linear depolarization to be approximately zero $\delta^{(m)} \approx 0$ and the lidar ratio to be approximately equal to $\mu^{(m)} \approx 20$. Second, based on the HSRL dust measurements we can approximate the dust lidar ratio to be $\mu^{(d)} \approx 35$ and depolarization to be $\delta^{(d)} \approx 0.3$. Third, based on the BACO tower in situ measurements, we can approximate the ratios between the dust/marine densities and cross-sectional areas by $N_d/N_m \approx 0.2$ and $A_h/A_d \approx (2/1.2)^2 \approx 2.7$.

With these approximations the reformulation of the expected depolarization ratio $\delta expected$ is

$$\delta expected \approx \frac{1.2}{4 + 94.5\chi} \quad (S17)$$

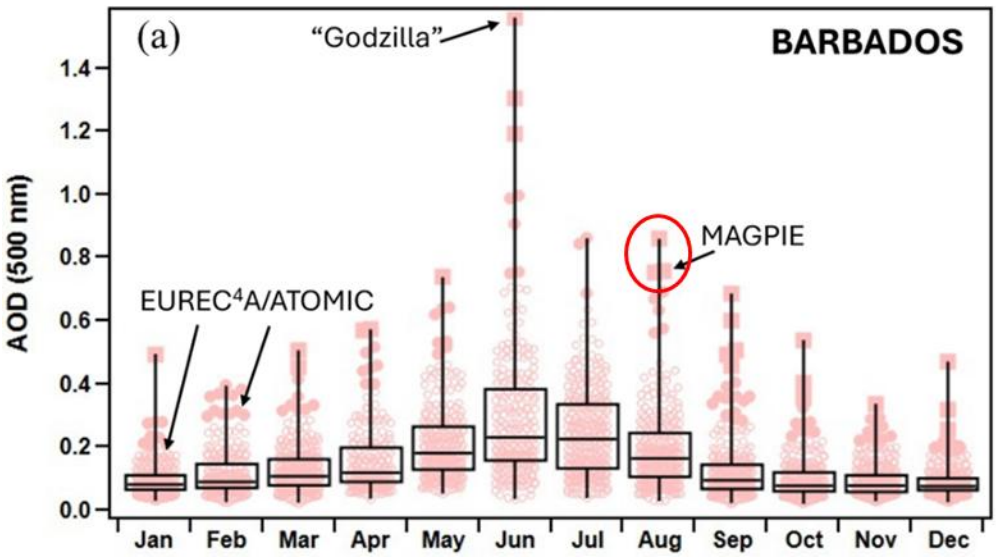

Figure S1. (a) Box plot showing monthly AOD at 500 nm measured using the AERONET (Holben et al., 1998) at Barbados for the last 17 years. AOD observed during MAGPIE are shown in red circle.

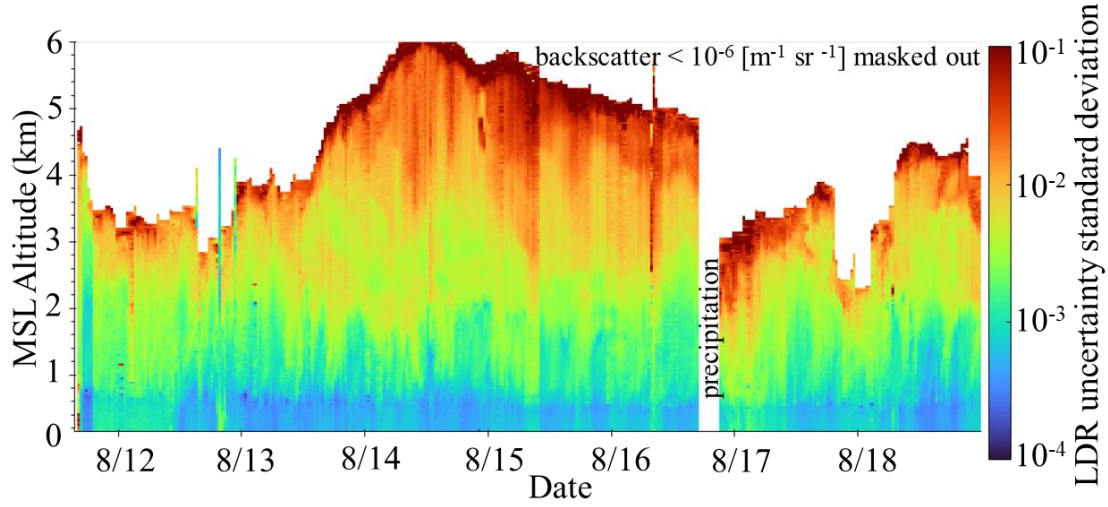

Figure S2. The systematic uncertainty standard deviation associated with the HSRL scan for particulate linear depolarization ratio (LDR; shown in Fig. 3b in main text) within 6 km above MSL for August 12 -18, 2023.

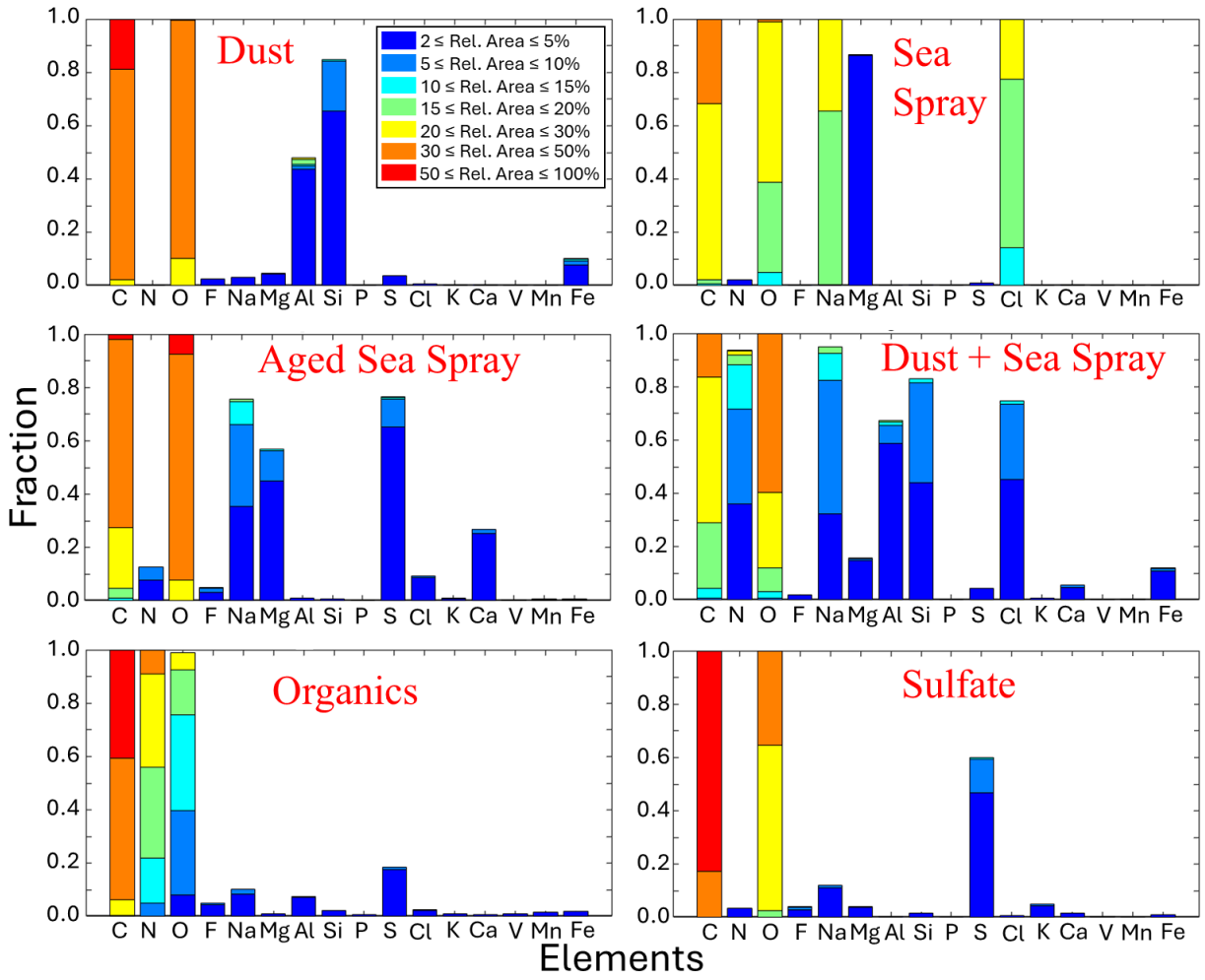

Figure S3. Digital color stack plots of CCSEM/EDX elemental spectra for representative ground-based particle clusters obtained after running the k-means clustering algorithm. The stacked bars illustrate the characteristic elemental signatures used to differentiate particle classes and the fraction of particles exhibiting each compositional pattern (e.g., Si, Al, Fe, Mg for mineral dust; Na, Cl, Mg for sea salt; S for aged or secondary species; C, O for organics).

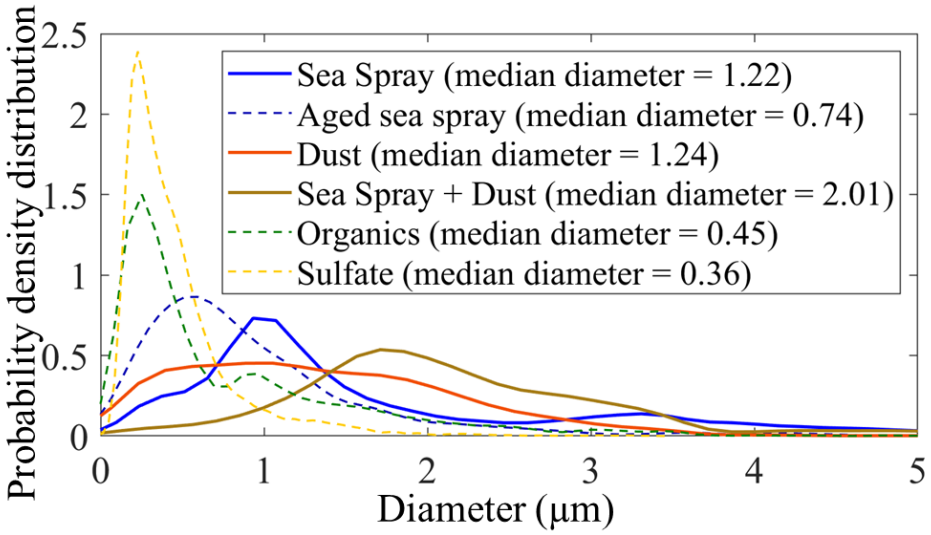

Figure S4. Probability density distribution of different particle types vs particle diameter during the dust event.

Table S1. Summary of CIRPAS Twin Otter airborne aerosol samples collected during the MAGPIE campaign.

Date	Time On [UTC]	Time Off [UTC]	MSL Altitude Sample taken [ft]	Cloud Base [ft]
13AUG23	15:02	15:30	100	2300
	16:35	16:50	2100	
14AUG23	14:50	15:08	10000	1800
	15:15	15:56	500	
15AUG23	15:30	15:37	3000	1000
	15:40	15:46	4500	
16AUG23	15:26	15:40	100 - 300	1500
	16:10	16:24	7000 - 9000	
18AUG23	14:35	15:00	100	1700
	16:53	17:10	4100	

Table S2. Statistical representation of airborne single-particle measurements showing the 95% confidence intervals for the number fractions of each aerosol particle type.

	Dust (%)	Dust + Sea Spray (%)	95% Confidence Interval[a]
SAL	0.90	0.10	±0.09
Above cloud top	0.57	0.43	±0.21
Below cloud base	0.42	0.58	±0.13

[a] Confidence intervals are calculated by assuming binomial statistics. For two complementary particle classes (i.e., dust and sea salt), the interval widths are identical because both are constrained by the same sampling variance term.

Table S3. List of Abbreviations

AERONET	AErosol RObotic NETwork
AOD	Aerosol Optical Depth
BACO	Barbados Atmospheric Chemistry Observatory
CBH	Cloud Base Height
CC/SEM	Computer-Controlled Scanning Electron Microscopy
CIMH	Caribbean Institute for Meteorology and Hydrology
CTO	CIRPAS Twin Otter aircraft
EMSL	Environmental Molecular Sciences Laboratory
IC	Ion Chromatography
LDR	Linear Depolarization Ratio
LR	Lidar Ratio
MABL	Marine Atmospheric Boundary Layer
MAGPIE	Moisture and Aerosol Gradients/Physics of Inversion Evolution
MPI	Max Planck Institute
MPS	Microanalysis Particle Sampler
NPS	Naval Postgraduate School
ONR	Office of Naval Research
PM	Particulate Matter

PNNL	Pacific Northwest National Laboratory
SAL	Saharan Air Layer
TSP	Total Suspended Particulate
SSEC	Space Science and Engineering Center
WHO	World Health Organization

References

Ault, A. P., Guasco, T. L., Ryder, O. S., Baltrusaitis, J., Cuadra-Rodriguez, L. A., Collins, D. B., Ruppel, M. J., Bertram, T. H., Prather, K. A., and Grassian, V. H.: Inside versus Outside: Ion Redistribution in Nitric Acid Reacted Sea Spray Aerosol Particles as Determined by Single Particle Analysis, J. Am. Chem. Soc., 135, 14528–14531, https://doi.org/10.1021/ja407117x, 2013a.

Ault, A. P., Zhao, D., Ebben, C. J., Tauber, M. J., Geiger, F. M., Prather, K. A., and Grassian, V. H.: Raman microspectroscopy and vibrational sum frequency generation spectroscopy as probes of the bulk and surface compositions of size-resolved sea spray aerosol particles, Phys. Chem. Chem. Phys., 15, 6206, https://doi.org/10.1039/c3cp43899f, 2013b.

Ault, A. P., Guasco, T. L., Baltrusaitis, J., Ryder, O. S., Trueblood, J. V., Collins, D. B., Ruppel, M. J., Cuadra-Rodriguez, L. A., Prather, K. A., and Grassian, V. H.: Heterogeneous Reactivity of Nitric Acid with Nascent Sea Spray Aerosol: Large Differences Observed between and within Individual Particles, J. Phys. Chem. Lett., 5, 2493–2500, https://doi.org/10.1021/jz5008802, 2014.

Chin, W.-C., Orellana, M. V., and Verdugo, P.: Spontaneous assembly of marine dissolved organic matter into polymer gels, Nature, 391, 568–572, https://doi.org/10.1038/35345, 1998.

Denjean, C., Caquineau, S., Desboeufs, K., Laurent, B., Maille, M., Quiñones Rosado, M., Vallejo, P., Mayol-Bracero, O. L., and Formenti, P.: Long-range transport across the Atlantic in summertime does not enhance the hygroscopicity of African mineral dust, Geophys. Res. Lett., 42, 7835–7843, https://doi.org/10.1002/2015GL065693, 2015.

Friehe, C. A. and Khelif, D.: Fast-Response Aircraft Temperature Sensors, J. Atmos. Ocean. Technol., 9, 784–795, https://doi.org/10.1175/1520-0426(1992)009<0784:FRATS>2.0.CO;2, 1992.

Gaston, C. J., Furutani, H., Guazzotti, S. A., Coffee, K. R., Bates, T. S., Quinn, P. K., Aluwihare, L. I., Mitchell, B. G., and Prather, K. A.: Unique ocean-derived particles serve as a proxy for changes in ocean chemistry, J. Geophys. Res., 116, D18310, https://doi.org/10.1029/2010JD015289, 2011.

Hand, V. L., Capes, G., Vaughan, D. J., Formenti, P., Haywood, J. M., and Coe, H.: Evidence of

internal mixing of African dust and biomass burning particles by individual particle analysis using electron beam techniques, J. Geophys. Res. Atmos., 115, https://doi.org/10.1029/2009JD012938, 2010.

Hänel, G.: Computation of the extinction of visible radiation by atmospheric aerosol particles as a function of the relative humidity, based upon measured properties, J. Aerosol Sci., 3, 377–386, https://doi.org/10.1016/0021-8502(72)90092-4, 1972.

Hänel, G.: The Single-Scattering Albedo of Atmospheric Aerosol Particles as a Function of Relative Humidity, J. Atmos. Sci., 33, 1120–1124, https://doi.org/10.1175/1520-0469(1976)033<1120:TSSAOA>2.0.CO;2, 1976.

Hegg, D. A., Covert, D. S., Jonsson, H., and Covert, P. A.: Determination of the Transmission Efficiency of an Aircraft Aerosol Inlet, Aerosol Sci. Technol., 39, 966–971, https://doi.org/10.1080/02786820500377814, 2005.

Holben, B. N., Eck, T. F., Slutsker, I., Tanré, D., Buis, J. P., Setzer, A., Vermote, E., Reagan, J. A., Kaufman, Y. J., Nakajima, T., Lavenu, F., Jankowiak, I., and Smirnov, A.: AERONET—A Federated Instrument Network and Data Archive for Aerosol Characterization, Remote Sens. Environ., 66, 1–16, https://doi.org/10.1016/S0034-4257(98)00031-5, 1998.

Kandler, K., Schneiders, K., Ebert, M., Hartmann, M., Weinbruch, S., Prass, M., and Pöhlker, C.: Composition and mixing state of atmospheric aerosols determined by electron microscopy: method development and application to aged Saharan dust deposition in the Caribbean boundary layer, Atmos. Chem. Phys., 18, 13429–13455, https://doi.org/10.5194/acp-18-13429-2018, 2018.

Krueger, B. J., Grassian, V. H., Cowin, J. P., and Laskin, A.: Heterogeneous chemistry of individual mineral dust particles from different dust source regions: the importance of particle mineralogy, Atmos. Environ., 38, 6253–6261, https://doi.org/10.1016/j.atmosenv.2004.07.010, 2004.

Levin, Z., Teller, A., Ganor, E., and Yin, Y.: On the interactions of mineral dust, sea-salt particles, and clouds: A measurement and modeling study from the Mediterranean Israeli Dust Experiment campaign, J. Geophys. Res. Atmos., 110, https://doi.org/10.1029/2005JD005810, 2005.

O'Dowd, C. D. and de Leeuw, G.: Marine aerosol production: a review of the current knowledge, Philos. Trans. R. Soc. A Math. Phys. Eng. Sci., 365, 1753–1774, https://doi.org/10.1098/rsta.2007.2043, 2007.

Reid, E. A., Reid, J. S., Meier, M. M., Dunlap, M. R., Cliff, S. S., Broumas, A., Perry, K., and Maring, H.: Characterization of African dust transported to Puerto Rico by individual particle and size segregated bulk analysis, J. Geophys. Res. Atmos., 108, https://doi.org/10.1029/2002JD002935, 2003.

Royer, H. M., Pöhlker, M. L., Krüger, O., Blades, E., Sealy, P., Lata, N. N., Cheng, Z., China, S., Ault, A. P., Quinn, P. K., Zuidema, P., Pöhlker, C., Pöschl, U., Andreae, M., and Gaston, C. J.: African smoke particles act as cloud condensation nuclei in the wintertime tropical North Atlantic boundary layer over Barbados, Atmos. Chem. Phys., 23, 981–998, https://doi.org/10.5194/acp-23-981-2023, 2023.

Royer, H. M., Sheridan, M. T., Elliott, H. E., Lata, N. N., Cheng, Z., China, S., Zhu, Z., Ault, A. P., and Gaston, C. J.: African dust transported to Barbados in the Wintertime Lacks Indicators of Chemical Aging, Atmos. Chem. Phys., https://doi.org/10.5194/egusphere-2024-3288, 2025.

Twohy, C. H., Kreidenweis, S. M., Eidhammer, T., Browell, E. V., Heymsfield, A. J., Bansemer, A. R., Anderson, B. E., Chen, G., Ismail, S., DeMott, P. J., and Van Den Heever, S. C.: Saharan dust particles nucleate droplets in eastern Atlantic clouds, Geophys. Res. Lett., 36, https://doi.org/10.1029/2008GL035846, 2009.